

Figure 2. Kaplan-Meier postoperative RFS and OS curves according to aromatase expression level. *N*, number of patients in each category. RFS (A) and OS (B) curves for all cohort patients. RFS (C) and OS (D) curves for females. RFS (E) and OS (F) curves for never-smokers. RFS (G) and OS (H) curves for patients with *EGFR* mutations.

and  $P = 0.07$  for OS; Supplementary Fig. S1E and S1F). Eleven patients with *EGFR* mutations had recurrent disease, and among them 8 patients received EGFR-TKI gefitinib after recurrence. There was no patient who received EGFR-TKI before recurrence.

Cox regression analyses for potential predictors of survival in patients with *EGFR* mutations are shown in Table 3. Among the parameters, aromatase expression and pathologic stage were identified as potential predictors of RFS. Multivariate analysis was not performed because of the small number of recurrences.

#### Growth inhibition of lung adenocarcinoma cell line by aromatase inhibitor

We examined aromatase mRNA expression in 21 human lung adenocarcinoma cell lines (Fig. 3A). No correlation was demonstrated between aromatase expression level and driver mutation type. Because patients with high aromatase expression had worse prognoses than those with low aromatase expression among those with *EGFR* mutations (Fig. 2G and H), we next investigated whether aromatase had therapeutic potential in lung adenocarcinomas with *EGFR* mutations. We chose 11-18 as high-aromatase mRNA-

**Table 2.** Cox proportion hazards model for RFS and OS ( $n = 110$ )

Variable	Univariate		Multivariate	
	HR (95% CI)	P	HR (95% CI)	P
<b>RFS</b>				
Age ( $\geq 70$ vs. $<70$ )	1.49 (0.71–3.17)	0.296		
Sex (male vs. female)	2.30 (1.09–5.06)	<b>0.029</b>	2.49 (1.13–5.74)	<b>0.024</b>
Smoking (current or former vs. never)	1.05 (0.49–2.21)	0.907		
<i>EGFR</i> mutation (positive vs. negative)	0.72 (0.32–1.51)	0.382		
Aromatase (high vs. low)	3.01 (1.35–6.64)	<b>0.008</b>	2.37 (1.05–5.31)	<b>0.039</b>
Pathologic stage ( $\geq$ II vs. I)	5.33 (2.53–11.5)	<b>&lt;0.001</b>	3.36 (1.50–7.70)	<b>0.003</b>
<b>OS</b>				
Age ( $\geq 70$ vs. $<70$ )	2.85 (1.06–8.97)	<b>0.041</b>		
Sex (male vs. female)	2.74 (1.04–7.97)	<b>0.038</b>		
Smoking (current or former vs. never)	0.76 (0.28–1.98)	0.573		
<i>EGFR</i> mutation (positive vs. negative)	0.25 (0.06–0.78)	<b>0.015</b>		
Aromatase (high vs. low)	4.20 (1.49–12.1)	<b>0.007</b>		
Pathologic stage ( $\geq$ II vs. I)	3.54 (1.35–9.46)	<b>0.011</b>		

NOTE: Multivariate analysis for OS was not performed because of the small number of events (deaths).

expressing cell line and HCC4006 as low-aromatase mRNA-expressing cell line, both of which have *EGFR* mutations. To test the growth inhibitory effects of the aromatase inhibitor exemestane, we conducted an MTT assay. HCC4006 was not sensitive to exemestane, either alone or combined with erlotinib (Fig. 3B). By contrast, 11-18 was sensitive to exemestane alone (Fig. 3C), and its cell growth was significantly inhibited by the combination of exemestane with erlotinib. We further tested the growth inhibitory effects of exemestane in high-aromatase mRNA-expressing cell lines without *EGFR* mutations: H358 (Supplementary Fig. S2A), H2228 (Supplementary Fig. S2B), and ACC-LC-319 (Supplementary Fig. S2C). The antitumor effect of exemestane in H358, H2228, and ACC-LC-319 was much weaker than in 11-18.

## Discussion

Although increasing evidence indicates that female hormones affect development of lung cancer (34–36), to our knowledge, this study is the first report to elucidate the prognostic significance of aromatase expression in patients

with lung adenocarcinomas with *EGFR* mutations. We found that aromatase mRNA expression level was not correlated with clinicopathologic factors, including *EGFR* mutation status. However, high aromatase expression was associated with poor prognosis in terms of both RFS and OS. Moreover, the prognostic significance of aromatase expression was limited to females, never-smokers, and patients with *EGFR* mutations, whereas such significance was not observed in their counterparts.

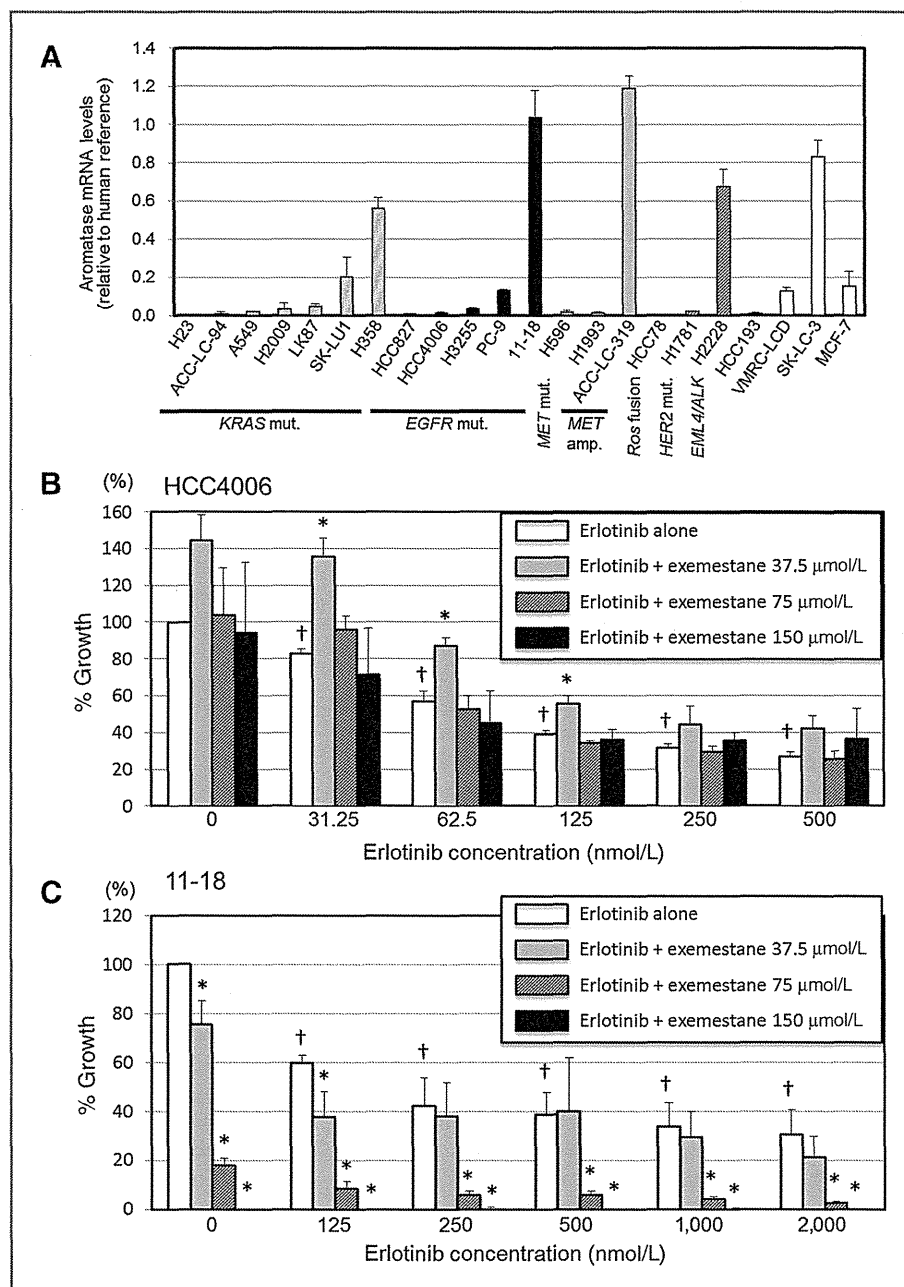
Aromatase is an enzyme that catalyzes the conversion from androgens to estrogens. In NSCLC cells, estrogen is reported to be mainly produced by intrinsic aromatase (23), and stimulates the ER signaling pathway, resulting in tumor development and progression (9–11, 13, 24). Here, we found that aromatase mRNA expression levels in carcinoma tissues were significantly higher than in corresponding nonneoplastic lung tissues. Niikawa and colleagues reported that the estradiol concentration in NSCLC was significantly higher than that in the nonneoplastic lung tissues, and intratumoral estradiol concentration in NSCLC was positively associated with aromatase mRNA expression

**Table 3.** Cox proportion hazards model for RFS in patients with *EGFR* mutations ( $n = 54$ )

Variable	Univariate	
	HR (95% CI)	P
Age: $\geq 70$ ( $n = 21$ ) vs. $<70$ ( $n = 33$ )	0.85 (0.22–2.82)	0.795
Sex: male ( $n = 12$ ) vs. female ( $n = 42$ )	3.48 (0.99–11.6)	0.050
Smoking: current/former ( $n = 15$ ) vs. never ( $n = 39$ )	1.60 (0.42–5.30)	0.466
Aromatase: high ( $n = 15$ ) vs. low ( $n = 39$ )	4.97 (1.50–19.0)	<b>0.009</b>
Pathologic stage: $\geq$ II ( $n = 13$ ) vs. I ( $n = 41$ )	6.55 (1.98–25.0)	<b>0.002</b>

NOTE: Multivariate analysis was not performed because of the small number of recurrences.

Figure 3. Effect of exemestane alone and in combination with erlotinib on *EGFR* mutant lung adenocarcinoma cell line proliferation. A, mRNA expression levels of aromatase in 21 human lung adenocarcinoma cell lines. Quantitative real-time RT-PCR was performed with validated TaqMan probes; assays were done in triplicate. The expression value for each cell line was calculated relative to that of human reference. MCF-7: breast carcinoma cell line. B, HCC4006 cells were not sensitive to exemestane alone or in combination with erlotinib. C, 11-18 cells were sensitive to exemestane alone and in combination with erlotinib. HCC4006 and 11-18 cells were incubated for 24 hours and for an additional 72 hours with the indicated concentrations of exemestane or erlotinib; cell growth was then measured. Independent experiments were repeated 3 times. \*,  $P < 0.05$  vs. erlotinib alone; †,  $P < 0.05$  vs. control (both erlotinib and exemestane were free) by Dunnett test. All data represent the mean  $\pm$  SD from 3 independent experiments.



(23). In another study, levels of aromatase activity tested by radioassay were significantly greater in tumors compared with those in nearby normal tissue (12). These studies indicate that intrinsic aromatase expression levels are closely associated with the estrogen levels in the lung cancer cells. Thus, increased aromatase level may have profound influence in carcinoma tissues through estrogen function.

Most estrogenic actions are mediated by ER, which exists in 2 forms, ER $\alpha$  and ER $\beta$  (37). Although immunohistochemical expressions of ER $\alpha$  and/or ER $\beta$  has been associated with clinical outcome in some studies (14–16, 26, 38),

the findings for expression frequency and subcellular localization (nuclear or cytoplasm) of ERs are inconsistent (14–16, 27, 36, 38, 39). These differences could be because of variation in such factors as (a) antibodies and dilutions, (b) scoring systems for staining, and (c) patient cohort characteristics (16). This discrepancy may obscure the significance of hormone receptor expression in patients' clinicopathologic characteristics or prognoses. For this reason, we found it difficult to clarify the effect of estrogen on the development of lung cancer using immunohistochemical analysis.

In this study, no significant correlation was identified between tumor aromatase expression and clinicopathologic factors, including *EGFR* mutations, when analyzed as either dichotomized or continuous variables. These results are consistent with previously reports (27, 39, 40). However, a correlation between *EGFR* mutation and ER expression, both ER $\alpha$  (14) and nuclear ER $\beta$  (15), in lung adenocarcinoma, was reported in previous studies, suggesting that some interaction between ER and the *EGFR* signaling pathway may exist.

High aromatase expression was associated with a poor prognosis in patients who underwent curative resections for lung adenocarcinoma. We also demonstrated that the prognostic significance of aromatase expression was limited to females, never-smokers, and patients with *EGFR* mutations, whereas such significance was not observed in their counterparts. We conducted Cox proportional hazards analysis in patients with *EGFR* mutations by RFS, not by OS, because 8 of 11 patients (73%) with *EGFR* mutations had received *EGFR*-TKI treatment for recurrence. *EGFR*-TKI prolonged the survival of such patients; therefore, the follow-up period may not have been enough to evaluate OS in this study. Aromatase expression level and *EGFR* mutation status did not directly correlate, but aromatase expression only held prognostic significance for lung adenocarcinomas with *EGFR* mutations, which suggests that estrogenic signaling augments growth that depends on the *EGFR* pathway. Mah and colleagues reported that lower aromatase levels predicted greater chances of survival in women 65 years and older with NSCLC, particularly among women who had no smoking history (13). Although they did not investigate *EGFR* mutation status, their results are consistent with ours. Nose and colleagues reported that strong nuclear expression of ER $\beta$  correlated with better disease-free survival in patients with *EGFR* mutations, but found no such prognostic significance in patients without *EGFR* mutations (15). They also suggested that strong ER $\beta$  expression was a surrogate marker for good response to *EGFR*-TKI (26). These results, along with our own, indicate that female hormone-related factors, such as aromatase and ER $\beta$ , affect outcomes only in lung adenocarcinomas with *EGFR* mutation, which suggests that hormonal and *EGFR* pathways may contribute in concert to progression of lung adenocarcinoma.

To investigate the influence of differences in aromatase expression between the tumor and normal tissues on patient survival, we classified patients into the following 2 groups: T > N, in whom aromatase expression in adenocarcinoma tissue was higher than in nonneoplastic lung tissue ( $n = 51$ ); and T < N, in whom it was lower ( $n = 43$ ). We performed survival analyses between the 2 groups, but saw no significant survival difference in RFS ( $P = 0.22$ ) or OS ( $P = 0.27$ ). We further compared RFS and OS between the 2 groups in subsets divided by sex, smoking history, and *EGFR* mutation status, but saw no significant difference in these analyses (data not shown).

Recently, interactions between the ER and *EGFR* pathways have been investigated *in vitro*. A nonnuclear ER pool

has been proposed that works via rapid signaling through various kinase cascades, including *EGFR* pathway and its downstream effectors in the lungs, such as MAPK (10, 11). However, the ER and *EGFR* pathways seem to act as alternate signaling pathways, with one upregulating when the other is inactivated (10, 41). This bi-directional crosstalk between ER and *EGFR* signaling suggests that simultaneous or combined therapy that targets both pathways could exert higher antitumor effect in patients with NSCLC.

Both *in vitro* and *in vivo* reports have demonstrated that estrogen downmodulator, alone or combined with *EGFR*-TKI, resulted in enhanced antitumor activity in NSCLCs (9–12, 23, 25, 41–44). Exemestane, an irreversible steroidal inactivator, either alone (41) or in combination with cisplatin (43) showed significant antitumor effects in 2 separate studies. Both letrozole and anastrozole, reversible steroidal inactivators, demonstrated similar antitumor activity in NSCLCs (12, 23, 44). However, lung cancer cell lines used in almost all of these studies were without *EGFR* mutations. We showed that the 11-18 cell line, which has an *EGFR* mutation accompanied with a high aromatase mRNA expression, was sensitive to exemestane alone and cell growth was significantly inhibited by the combination of exemestane and erlotinib. We also demonstrated that exemestane's antitumor effects in H358, H2228, and ACC-LC-319, which have high aromatase expressions without *EGFR* mutations, were much weaker than in 11-18. These results suggest that sensitivity to the aromatase inhibitor may depend on crosstalk between ER and the *EGFR* pathway; reducing estrogenic signaling by inhibiting aromatase might inhibit cell growth that depends on the *EGFR* pathway. Therefore, our result suggests that selecting patients with high aromatase expression accompanied by *EGFR* mutation might improve clinical responses to the combination of *EGFR*-TKI and aromatase inhibitor. However, we tested the growth inhibitory effects of only one cell line with high aromatase expression and *EGFR* mutation, thus this study remains limited. Further studies using *in vivo* and clinical models are needed to elucidate the therapeutic potential of aromatase inhibitor in lung adenocarcinomas with *EGFR* mutations. Traynor and colleagues reported a pilot study of gefitinib and fulvestrant in the treatment of 22 postmenopausal women diagnosed as NSCLC (45). No significant results were obtained in this small study, but combination therapy was well tolerated. Three of 12 patients tested for *EGFR* mutation status detected *EGFR* mutation. A trial of *EGFR*-TKI and estrogen downmodulator in patients with NSCLC with *EGFR* mutations may be therefore needed in the future.

In conclusion, high aromatase expression is correlated with poor outcome in patients with lung adenocarcinoma, including those with *EGFR* mutations. Aromatase may be a useful therapeutic target in lung adenocarcinomas with high aromatase expression and *EGFR* mutations. Although our results provide potential insights into the influence of aromatase expression in lung cancer, further studies are required to better understand the

mechanisms of aromatase expression and interaction with *EGFR* signaling, and to determine the clinical applicability of aromatase inhibitors.

#### Disclosure of Potential Conflicts of Interest

Y. Maehara reports receiving other research grants from Chugai and Pfizer. No potential conflicts of interest were disclosed by the other authors.

#### Authors' Contributions

**Conception and design:** M. Kohno, T. Okamoto, K. Suda  
**Development of methodology:** M. Kohno, K. Suda, T. Yano  
**Acquisition of data (provided animals, acquired and managed patients, provided facilities, etc.):** M. Kohno, T. Yano  
**Analysis and interpretation of data (e.g., statistical analysis, biostatistics, computational analysis):** M. Kohno, K. Suda, M. Shimokawa  
**Writing, review, and/or revision of the manuscript:** M. Kohno, T. Okamoto, M. Shimokawa, M. Takenoyama, T. Yano

**Administrative, technical, or material support (i.e., reporting or organizing data, constructing databases):** K. Suda, H. Kitahara, S. Shimamatsu, H. Konishi, T. Yoshida

**Study supervision:** M. Takenoyama, T. Yano, Y. Maehara

#### Acknowledgments

The authors thank Dr. A.F. Gazdar, Dr. T. Hida, Dr. K. Tomizawa, Dr. T. Mitsudomi, and Dr. M. Takeshita for kindly providing cell lines.

#### Grant Support

This study was supported in part by a Grant-in-Aid for Scientific Research (C) from the Japan Society for the Promotion of Science (21591816).

The costs of publication of this article were defrayed in part by the payment of page charges. This article must therefore be hereby marked *advertisement* in accordance with 18 U.S.C. Section 1734 solely to indicate this fact.

Received September 30, 2013; revised April 13, 2014; accepted April 14, 2014; published OnlineFirst May 6, 2014.

#### References

- Jemal A, Bray F, Center MM, Ferlay J, Ward E, Forman D. Global cancer statistics. *CA Cancer J Clin* 2011;61:69–90.
- Sun S, Schiller JH, Gazdar AF. Lung cancer in never smokers—a different disease. *Nat Rev Cancer* 2007;7:778–90.
- Yano T, Miura N, Takenaka T, Haro A, Okazaki H, Ohba T, et al. Never-smoking nonsmall cell lung cancer as a separate entity: clinicopathologic features and survival. *Cancer* 2008;113:1012–8.
- Yano T, Haro A, Shikada Y, Maruyama R, Maehara Y. Non-small cell lung cancer in never smokers as a representative 'non-smoking-associated lung cancer': epidemiology and clinical features. *Int J Clin Oncol* 2011;16:287–93.
- Shigematsu H, Lin L, Takahashi T, Nomura M, Suzuki M, Wistuba II, et al. Clinical and biological features associated with epidermal growth factor receptor gene mutations in lung cancers. *J Natl Cancer Inst* 2005;97:339–46.
- Kosaka T, Yatabe Y, Endoh H, Kuwano H, Takahashi T, Mitsudomi T. Mutations of the epidermal growth factor receptor gene in lung cancer: biological and clinical implications. *Cancer Res* 2004;64:8919–23.
- Shaw AT, Yeap BY, Mino-Kenudson M, Digumarthy SR, Costa DB, Heist RS. Clinical features and outcome of patients with non-small-cell lung cancer who harbor *EML4-ALK*. *J Clin Oncol* 2009;27:4247–53.
- Patrone C, Cassel TN, Pettersson K, Piao YS, Cheng G, Ciana P, et al. Regulation of postnatal lung development and homeostasis by estrogen receptor  $\beta$ . *Mol Cell Biol* 2003;23:8542–52.
- Stabile LP, Davis AL, Gubish CT, Hopkins TM, Luketich JD, Christie N, et al. Human non-small cell lung tumors and cells derived from normal lung express both estrogen receptor  $\alpha$  and  $\beta$  and show biological responses to estrogen. *Cancer Res* 2002;62:2141–50.
- Stabile LP, Lyker JS, Gubish CT, Zhang W, Grandis JR, Siegfried JM. Combined targeting of the estrogen receptor and the epidermal growth factor receptor in non-small cell lung cancer shows enhanced antiproliferative effects. *Cancer Res* 2005;65:1459–70.
- Pietras RJ, Marquez DC, Chen HW, Tsai E, Weinberg O, Fishbein M. Estrogen and growth factor receptor interactions in human breast and non-small cell lung cancer cells. *Steroids* 2005;70:372–81.
- Weinberg OK, Marquez-Garban DC, Fishbein MC, Goodglick L, Garban HJ, Dubinett SM, et al. Aromatase inhibitors in human lung cancer therapy. *Cancer Res* 2005;65:11287–91.
- Mah V, Seligson DB, Li A, Márquez DC, Wistuba II, Elshimali Y, et al. Aromatase expression predicts survival in women with early-stage non-small cell lung cancer. *Cancer Res* 2007;67:10484–90.
- Raso MG, Behrens C, Herynk MH, Liu S, Prudkin L, Ozburn NC, et al. Immunohistochemical expression of estrogen and progesterone receptors identifies a subset of NSCLCs and correlates with *EGFR* mutation. *Clin Cancer Res* 2009;15:5359–68.
- Nose N, Sugio K, Oyama T, Nozoe T, Uramoto H, Iwata T, et al. Association between estrogen receptor- $\beta$  expression and epidermal growth factor receptor mutation in the postoperative prognosis of adenocarcinoma of the lung. *J Clin Oncol* 2009;27:411–7.
- Stabile LP, Dacic S, Land SR, Lenzner DE, Dhir R, Acquafondata M, et al. Combined analysis of estrogen receptor  $\beta$ -1 and progesterone receptor expression identifies lung cancer patients with poor outcome. *Clin Cancer Res* 2011;17:154–64.
- Liu Y, Inoue M, Sobue T, Tsugane S. Reproductive factors, hormone use and the risk of lung cancer among middle-aged never-smoking Japanese women: a large-scale population-based cohort study. *Int J Cancer* 2005;117:662–6.
- Chlebowski RT, Schwartz AG, Wakelee H, Anderson GL, Stefanick ML, Manson JE, et al. Oestrogen plus progestin and lung cancer in postmenopausal women (Women's Health Initiative trial): a post-hoc analysis of a randomised controlled trial. *Lancet* 2009;374:1243–51.
- Slatore CG, Chien JW, Au DH, Satia JA, White E. Lung cancer and hormone replacement therapy: association in the vitamins and lifestyle study. *J Clin Oncol* 2010;28:1540–6.
- Coombes RC, Hall E, Gibson LJ, Paridaens R, Jassem J, Delozier T, et al. A randomized trial of exemestane after two to three years of tamoxifen therapy in postmenopausal women with primary breast cancer. *N Engl J Med* 2004;350:1081–92.
- Simpson ER, Mahendroo MS, Means GD, Kilgore MW, Hinshelwood MM, Graham-Lorence S, et al. Aromatase cytochrome P450, the enzyme responsible for estrogen biosynthesis. *Endocr Rev* 1994;15:342–55.
- Smith IE, Dowsett M. Aromatase inhibitors in breast cancer. *N Engl J Med* 2003;348:2431–42.
- Niikawa H, Suzuki T, Miki Y, Suzuki S, Nagasaki S, Akahira J, et al. Intratumoral estrogens and estrogen receptors in human non-small cell lung carcinoma. *Clin Cancer Res* 2008;14:4417–26.
- Hershberger PA, Stabile LP, Kanterewicz B, Rothstein ME, Gubish CT, Land S, et al. Estrogen receptor  $\beta$  (ER $\beta$ ) subtype-specific ligands increase transcription, p44/p42 mitogen activated protein kinase (MAPK) activation and growth in human non-small cell lung cancer cells. *J Steroid Biochem Mol Biol* 2009;116:102–9.
- Garon EB, Pietras RJ, Finn RS, Kamranpour N, Pitts S, Márquez-Garban DC, et al. Antiestrogen fulvestrant enhances the antiproliferative effects of epidermal growth factor receptor inhibitors in human non-small-cell lung cancer. *J Thorac Oncol* 2013;8:270–8.
- Nose N, Uramoto H, Iwata T, Hanagiri T, Yasumoto K. Expression of estrogen receptor  $\beta$  predicts a clinical response and longer progression-free survival after treatment with *EGFR*-TKI for adenocarcinoma of the lung. *Lung Cancer* 2011;71:350–5.
- Sun HB, Zheng Y, Ou W, Fang Q, Li P, Ye X, et al. Association between hormone receptor expression and epidermal growth factor receptor

- mutation in patients operated on for non-small cell lung cancer. *Ann Thorac Surg* 2011;91:1562-7.
28. Travis WD, Brambilla E, Muller-Hermelink HK, Harris CC. Tumours of the lung, pleura, thymus and heart. Pathology and genetics. Lyon: IARC Press; 2004.
  29. Goldstraw P, Crowley J, Chansky K, Giroux DJ, Groome PA, Rami-Porta R, et al. International Association for the Study of Lung Cancer International Staging Committee; Participating Institutions. The IASLC Lung Cancer Staging Project: proposals for the revision of the TNM stage groupings in the forthcoming (seventh) edition of the TNM Classification of Malignant Tumours. *J Thorac Oncol* 2007; 2:706-14.
  30. Nagai Y, Miyazawa H, Huqun, Tanaka T, Udagawa K, Kato M, et al. Genetic heterogeneity of the epidermal growth factor receptor in non-small cell lung cancer cell lines revealed by a rapid and sensitive detection system, the peptide nucleic acid-locked nucleic acid PCR clamp. *Cancer Res* 2005;65:7276-82.
  31. Suda K, Tomizawa K, Fujii M, Murakami H, Osada H, Maehara Y, et al. Epithelial to mesenchymal transition in an epidermal growth factor receptor-mutant lung cancer cell line with acquired resistance to erlotinib. *J Thorac Oncol* 2011;6:1152-61.
  32. Tomizawa K, Suda K, Onozato R, Kuwano H, Yatabe Y, Mitsudomi T. Analysis of ERBB4 mutations and expression in Japanese patients with lung cancer. *J Thorac Oncol* 2010;5:1859-61.
  33. Suda K, Murakami I, Katayama T, Tomizawa K, Osada H, Sekido Y, et al. Reciprocal and complementary role of MET amplification and EGFR T790M mutation in acquired resistance to kinase inhibitors in lung cancer. *Clin Cancer Res* 2010;16:5489-98.
  34. Siegfried JM, Hershberger PA, Stabile LP. Estrogen receptor signaling in lung cancer. *Semin Oncol* 2009;36:524-31.
  35. Verma MK, Miki Y, Sasano H. Aromatase in human lung carcinoma. *Steroids* 2011;76:759-64.
  36. Miki Y, Abe K, Suzuki S, Suzuki T, Sasano H. Suppression of estrogen actions in human lung cancer. *Mol Cell Endocrinol* 2011;340:168-74.
  37. Cheng G, Weihua Z, Warner M, Gustafsson JA. Estrogen receptors ER  $\alpha$  and ER  $\beta$  in proliferation in the rodent mammary gland. *Proc Natl Acad Sci U S A* 2004;101:3739-46.
  38. Ishibashi H, Suzuki T, Suzuki S, Niikawa H, Lu L, Miki Y, et al. Progesterone receptor in non-small cell lung cancer—a potent prognostic factor and possible target for endocrine therapy. *Cancer Res* 2005;65:6450-8.
  39. Abe K, Miki Y, Ono K, Mori M, Kakinuma H, Kou Y, et al. Highly concordant coexpression of aromatase and estrogen receptor  $\beta$  in non-small cell lung cancer. *Hum Pathol* 2010;41:190-8.
  40. Oyama T, Kagawa N, Sugio K, Uramoto H, Hatano O, Harada N, et al. Expression of aromatase CYP19 and its relationship with parameters in NSCLC. *Front Biosci* 2009;14:2285-92.
  41. Koutras A, Giannopoulou E, Kritikou I, Antonacopoulou A, Evans TR, Papavas-siliou AG, et al. Antiproliferative effect of exemestane in lung cancer cells. *Mol Cancer* 2009;24:109.
  42. Marquez-Garban DC, Chen HW, Fishbein MC, Goodglick L, Pietras RJ. Estrogen receptor signaling pathways in human non-small cell lung cancer. *Steroids* 2007;72:135-43.
  43. Márquez-Garbán DC, Chen HW, Goodglick L, Fishbein MC, Pietras RJ. Targeting aromatase and estrogen signaling in human non-small cell lung cancer. *Ann NY Acad Sci* 2009;1155:194-205.
  44. Miki Y, Suzuki T, Abe K, Suzuki S, Niikawa H, Iida S, et al. Intratumoral localization of aromatase and interaction between stromal and parenchymal cells in the non-small cell lung carcinoma microenvironment. *Cancer Res* 2010;70:6659-69.
  45. Traynor AM, Schiller JH, Stabile LP, Kolesar JM, Eickhoff JC, Dacic S, et al. Pilot study of gefitinib and fulvestrant in the treatment of postmenopausal women with advanced non-small cell lung cancer. *Lung Cancer* 2009;64:51-9.

# Clinical Cancer Research

## Prognostic and Therapeutic Implications of Aromatase Expression in Lung Adenocarcinomas with *EGFR* Mutations

Mikihiro Kohno, Tatsuro Okamoto, Kenichi Suda, et al.

*Clin Cancer Res* 2014;20:3613-3622. Published OnlineFirst May 6, 2014.

**Updated version** Access the most recent version of this article at:  
[doi:10.1158/1078-0432.CCR-13-2683](https://doi.org/10.1158/1078-0432.CCR-13-2683)

**Supplementary Material** Access the most recent supplemental material at:  
<http://clincancerres.aacrjournals.org/content/suppl/2014/05/07/1078-0432.CCR-13-2683.DC1.html>

**Cited Articles** This article cites by 44 articles, 18 of which you can access for free at:  
<http://clincancerres.aacrjournals.org/content/20/13/3613.full.html#ref-list-1>

**Citing articles** This article has been cited by 1 HighWire-hosted articles. Access the articles at:  
<http://clincancerres.aacrjournals.org/content/20/13/3613.full.html#related-urls>


**E-mail alerts** Sign up to receive free email-alerts related to this article or journal.

**Reprints and Subscriptions** To order reprints of this article or to subscribe to the journal, contact the AACR Publications Department at [pubs@aacr.org](mailto:pubs@aacr.org).

**Permissions** To request permission to re-use all or part of this article, contact the AACR Publications Department at [permissions@aacr.org](mailto:permissions@aacr.org).

# Correlation between whole tumor size and solid component size on high-resolution computed tomography in the prediction of the degree of pathologic malignancy and the prognostic outcome in primary lung adenocarcinoma

Hisashi Saji<sup>1,4</sup>, Jun Matsubayashi<sup>2</sup>, Soichi Akata<sup>3</sup>, Yoshihisa Shimada<sup>1</sup>, Yasufumi Kato<sup>1</sup>, Yujin Kudo<sup>1</sup>, Toshitaka Nagao<sup>2</sup>, Jinho Park<sup>3</sup>, Masatoshi Kakihana<sup>1</sup>, Naohiro Kajiwara<sup>1</sup>, Tatsuo Ohira<sup>1</sup> and Norihiko Ikeda<sup>1</sup>

Acta Radiologica  
0(0) 1–9  
© The Foundation Acta Radiologica  
2014  
Reprints and permissions:  
sagepub.co.uk/journalsPermissions.nav  
DOI: 10.1177/0284185114554823  
acr.sagepub.com  


## Abstract

**Background:** The presence of ground glass opacity (GGO) on high-resolution computed tomography (HRCT) is well known to be pathologically closely associated with adenocarcinoma in situ.

**Purpose:** To determine whether it is more useful to evaluate the whole tumor size or only the solid component size to predict the pathologic high-grade malignancy and the prognostic outcome in lung adenocarcinoma.

**Material and Methods:** Using HRCT data of 232 patients with adenocarcinoma who underwent curative resection, we retrospectively measured the whole tumor and solid component sizes with lung window setting (WTLW and SCLW) and whole tumor sizes with a mediastinal window setting (WTMW).

**Results:** There was significant correlation between the WTLW and the measurements of pathological whole tumor (pWT) ( $r=0.792$ ,  $P<0.0001$ ). The SCLW and WTLW values significantly correlated with the area of pathological invasive component (pIVS) ( $r=0.762$ ,  $P<0.0001$  and  $r=0.771$ ,  $P<0.0001$ , respectively). The receiver operating characteristics area under the curve for WTLW, SCLW, and WTMW used to identify lymph node metastasis or lymphatic or vascular invasion were 0.693, 0.817, and 0.824, respectively. Kaplan-Meier curves of disease-free survival (DFS) and overall survival (OS) were better divided according to SCLW and WTMW, compared with WTLW. Multivariate analysis of DFS and OS revealed that WTMW was an independent prognostic factor (HR=0.72, 95% confidence interval [CI]=0.58–0.90,  $P=0.004$  and HR=0.74, 95% CI=0.57–0.96,  $P=0.022$ , respectively).

**Conclusion:** The predictive values of the solid tumor size visualized on HRCT especially in the mediastinal window for pathologic high-grade malignancy and prognosis in lung adenocarcinoma were greater than those of whole tumor size.

## Keywords

Lung adenocarcinoma, prognosis, solid component, ground glass nodule, high-resolution computed tomography

Date received: 19 May 2014; accepted: 17 September 2014

## Introduction

The National Lung Screening Trial demonstrated a significant reduction in mortality from lung cancer with low-dose CT screening of 20.0% (95% confidence interval [CI], 6.8–26.7;  $P=0.004$ ) (1). Recent advances in

<sup>1</sup>Department of Thoracic Surgery, Tokyo Medical University, Tokyo, Japan

<sup>2</sup>Department of Anatomic Pathology, Tokyo Medical University, Tokyo, Japan

<sup>3</sup>Department of Radiology, Tokyo Medical University, Tokyo, Japan

<sup>4</sup>Department of Chest Surgery, St. Marianna University School of Medicine, Kanagawa, Japan

## Corresponding author:

Hisashi Saji, MD, PhD Associate Professor Department of Chest Surgery, St. Marianna University School of Medicine 2-16-1 Sugao, Miyamae-ku, Kawasaki, Kanagawa 216-8511, Japan.  
Email: saji-q@ya2.so-net.ne.jp



high-resolution computed tomography (HRCT) and the widespread application of CT screening due to the positive results of screening CT trial have enhanced the discovery of small lung cancers, particularly adenocarcinoma (1). These often contain a non-solid component that presents as ground glass opacity (GGO) features on HRCT. Several investigators have reported that GGO is closely associated with bronchioloalveolar carcinoma (BAC) (2).

Recently, the International Association for the Study of Lung Cancer, the American Thoracic Society, and the European Respiratory Society proposed a new classification of lung adenocarcinoma. The terms BAC and mixed subtype adenocarcinoma are no longer used. For resected specimens, new concepts have been introduced such as adenocarcinoma in situ (AIS) and minimally invasive adenocarcinoma (MIA) for small solitary adenocarcinomas with either pure lepidic growth: AIS or predominantly lepidic growth with 5 mm invasion and MIA to define patients who, if they undergo complete resection, will have 100% or near 100% disease-specific survival rates, respectively (3,4). We therefore hypothesized that the GGO component is not related to malignancy or prognosis, implying that only the solid component of the tumor on HRCT (solid tumor size) is indicative of malignancy and prognosis in lung adenocarcinoma.

In this study, we first compared the whole tumor and solid component size, excluding areas of GGO, on preoperative HRCT with a lung window setting and whole tumor size with a mediastinal window setting with pathological whole tumor size and the area of pathologically confirmed invasion. We then determined whether it is more useful to evaluate the whole tumor size or that of only the solid component size to predict the degree of malignancy including lymph node involvement, lymphatic invasion, or vascular invasion of tumors in lung adenocarcinoma.

## Material and Methods

### Patients

Using preoperative HRCT data of 277 consecutive patients with adenocarcinoma who underwent curative surgical resection from January 2005 to December 2007, we retrospectively measured the whole tumor size and solid component size as follows: the whole tumor and solid component size was measured with lung window setting (WTLW and SCLW) and whole tumor size, with a mediastinal window setting (WTMW) on HRCT. Staging was determined according to the 7th edition of the TNM staging system (5). The histological tumor type was determined according to the World Health Organization (WHO) classification, 3rd edition.

In addition, we measured the maximum size of the area pathologically confirmed invasion for this study. We excluded 21 patients with adenocarcinoma with scattered invasive components for this analysis, due to difficulty in measuring not only the pathological invasive area but also the size of the solid component radiologically. Twenty-four patients with inappropriate tissue samples were also excluded following induction therapy or divided tumor resection due to intraoperative frozen diagnosis. Ultimately, 232 consecutive patients with adenocarcinomas were enrolled in this study. Radiological and pathological findings were conducted by SA and JP, and JM and TN, respectively, who were blinded from any clinical information.

Patients were examined at 3-month intervals for the first 2 years and at 6-month intervals for the next 3 years and thereafter on an outpatient basis. The follow-up evaluation involved the following procedures: physical examination, chest radiography, CT of the chest and abdomen, and blood examination, including that of pertinent tumor markers. Further evaluations, including brain magnetic resonance imaging or CT, bone scintigraphy and integrated positron emission tomography, were performed on the first appearance of any symptom or sign of recurrence. The median follow-up time of this series was 4.4 years.

### HRCT scanning

Chest images were obtained using 64-detector row CT scanners (LightSpeed VCT: GE Healthcare, Milwaukee, WI, USA and SOMATOM Sensation Cardiac 64: Siemens Medical Systems, Erlangen, Germany) and a 16-detector row CT scanner (BrightSpeed Elite: GE Healthcare, Milwaukee, WI, USA). High-resolution images of the tumors were acquired using the following parameters: 120 kV and auto exposure control; collimation, 0.6–1.25 mm; pitch, 0.9–0.984; 0.4–0.5 s per rotation; reconstructed interval, 1.25–1.5 mm; pixel resolution, 512 × 512; field of view, 20 cm; and a lung window settings (level = -500/width = 1500 HU) with high spatial frequency algorithm and mediastinal window settings (level = 40/width = 320 HU) with soft-tissue algorithm. GGO was defined as an increase in lung attenuation that did not obscure the underlying vascular markings. We defined the solid tumor size as the maximum dimension of the solid component of the lung windows excluding GGO (SCLW) or the maximum dimension of the whole tumor size of mediastinal setting (WTMW) (Fig. 1a and b).

### Pathological findings

Histopathological studies were performed according to WHO criteria, 3rd edition (6). All resected

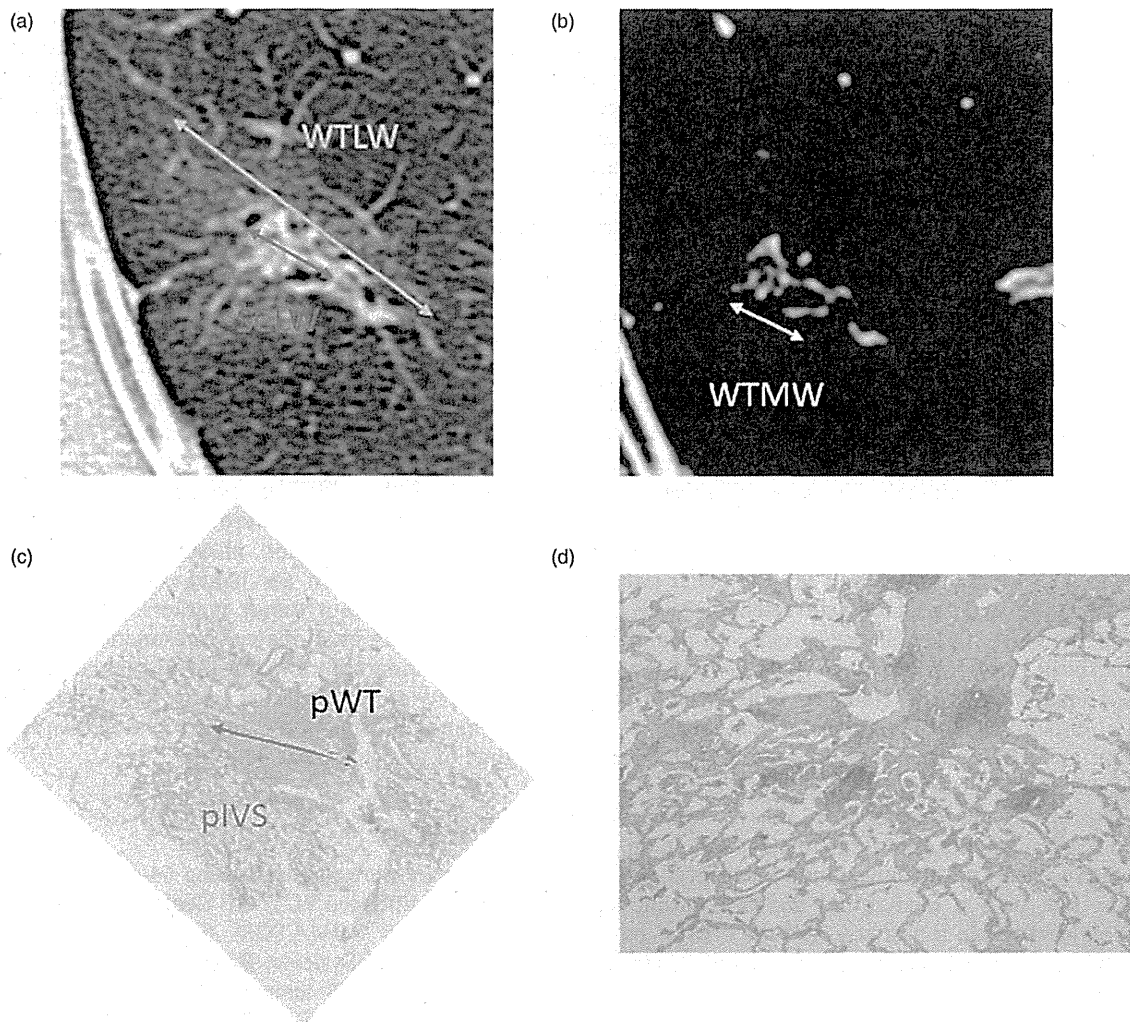


**Fig. 1.** Correlation between radiological and pathological findings in one typical case. WTLW and SCLW (a), WTMW (b), pWT and pIVS (c), pathological invasive area with high magnification (d). pIVS, pathologically confirmed invasion size; pWT, pathologically confirmed whole tumor size; SCLW, solid component size of lung windows setting; WTLW, whole tumor size of lung windows setting; WTMW, whole tumor size of mediastinal setting.

specimens were formalin-fixed and stained with hematoxylin and eosin in the routine manner. For detailed examinations of lymphatic or vascular invasion or pleural invasion, Elastica van Gieson stain was used to evaluate histological structure and tumor invasion. We also assessed several histological factors: (i) pathological nodal status (pN); (ii) vascular (v) or lymphatic (ly) invasion; and (iii) degree of tumor differentiation (well [G1], moderate [G2], poor [G3]). The maximum size of the pathological whole tumor (pWT) and of the pathological invasive component were measured (pIVS). The maximum size of pWT was assessed by standard gross measurement or histological reconstruction, as necessary. The maximum

size of the invasive component was measured microscopically. If the tumor was large, the maximum size of the invasive area was calculated by reconstruction of the tumor slides and measured (Fig. 1c and d). Pathologic high-grade malignancy was defined as lymph node involvement, lymphatic invasion, or vascular invasion.

#### Statistical analysis

The data are presented as numbers and percentages or mean  $\pm$  standard deviation, unless otherwise stated. The receiver operating characteristic curves of the whole and solid tumor sizes were used for the

**Table 1.** Radiological and pathological findings of 232 patients with lung adenocarcinoma.

Variables	n (% or range)	
Radiological findings		
WTLW: mean $\pm$ SD (cm)	2.59 $\pm$ 1.09 (0.73–6.84)	
SCLW: mean $\pm$ SD (cm)	2.01 $\pm$ 1.18 (0.00–5.78)	
WTMW: mean $\pm$ SD (cm)	1.87 $\pm$ 1.18 (0.00–5.71)	
Pathological findings		
pT status: pT1a / pT1b / pT2a / pT2b / pT3	86 (37.2) / 68 (29.2) / 61 (26.2) / 6 (2.7) / 11 (4.7)	
pN status: pN0 / pN1 / pN2	195 (83.7) / 20 (8.6) / 17 (7.7)	
pStage: pIA / pIB / pIIA / pIIB / pIIIA	141 (60.5) / 48 (20.6) / 8(3.4) / 8 (3.4) / 27 (12.1)	
pWT: mean $\pm$ SD, cm	2.61 $\pm$ 1.11 (0.90–7.20)	
pIVS: mean $\pm$ SD, cm	2.26 $\pm$ 1.27 (0.00–7.2)	
Differentiated: well or poorly	118 (50.6) / 107 (45.9)	ND: 8
Ly: positive / negative	127 (54.5) / 102 (43.8)	ND: 3
V: positive / negative	82 (35.2) / 150 (64.8)	

Ly, lymphatic invasion; ND, no data; pIVS, pathological invasion size; pN, pathological nodal status; pT, pathological T status; pWT, pathological whole tumor size; SCLW, solid component size of lung windows setting; V, vascular invasion; WTLW, whole tumor size of lung windows setting; WTMW, whole tumor size of mediastinal setting.

prediction of lymph node involvement, lymphatic invasion, or vascular invasion or well differentiation. We also performed multiple logistic regression analysis to determine the independent variables related to the whole tumor size and the solid tumor size for the prediction of the pathologic finding of high-grade malignancy. Overall survival (OS) was calculated from the date of surgery to the time of death. Observations were censored at final follow-up if the patient was living. Disease-free survival (DFS) was defined as the interval from the date of surgery until the first event (relapse or death from any cause) or the last follow-up visit. The duration of DFS was analyzed using the Kaplan-Meier method. Differences in OS or DFS were assessed using the log-rank test. To assess the potential independent and valuable prognostic effects of clinical tumor size on OS or DFS, we performed multivariate analysis with the Cox proportional hazards model using variables with  $P < 0.05$ . The data were statistically analyzed using the Statistical Package for Social Sciences software, version 10.5 (SPSS Inc., Chicago, IL, USA).

#### Ethical considerations

The approval of the Institutional Review Board of Tokyo Medical University was obtained (project approval No. 1665), but as this was a retrospective study the need to obtain written informed consent from either the patients or their representatives was waived, in accordance with the American Medical Association Manual of Style (10th edition).

## Results

### Patient characteristics

There were 118 (51.0%) women and 114 (49.0%) men aged 35–86 years (mean, 65.0 years). The several radiological and pathological findings of 232 patients are summarized in Table 1.

### Correlation between radiological and pathological findings

Fig. 2 shows several correlations between radiological findings including WTLW, SCLW, or WTMW, and pathological findings including pWT or pIVS. There were significant correlations between SCLW and pIVS ( $R = 0.762$ , 95% CI = 0.702–0.811,  $P < 0.0001$ ), WTMW and pIVS ( $R = 0.771$ , 95% CI = 0.713–0.819,  $P < 0.0001$ ), and WTLW and pIVS ( $R = 0.792$ , 95% CI = 0.735–0.835,  $P < 0.0001$ ), respectively.

### Receiver operating characteristic curve

The receiver operating characteristic area under the curve values of WTLW, SCLW, WTMW, and pIVS used for predicting lymph node involvement, lymphatic invasion, vascular invasion, degree of differentiation, and pathologic high-grade malignancy (lymph node involvement or lymphatic or vascular invasion) are given in Table 2 and Fig. 3. The predictability of all outcomes on the basis of solid tumor size such as SCLW and WTMW was better than that using the

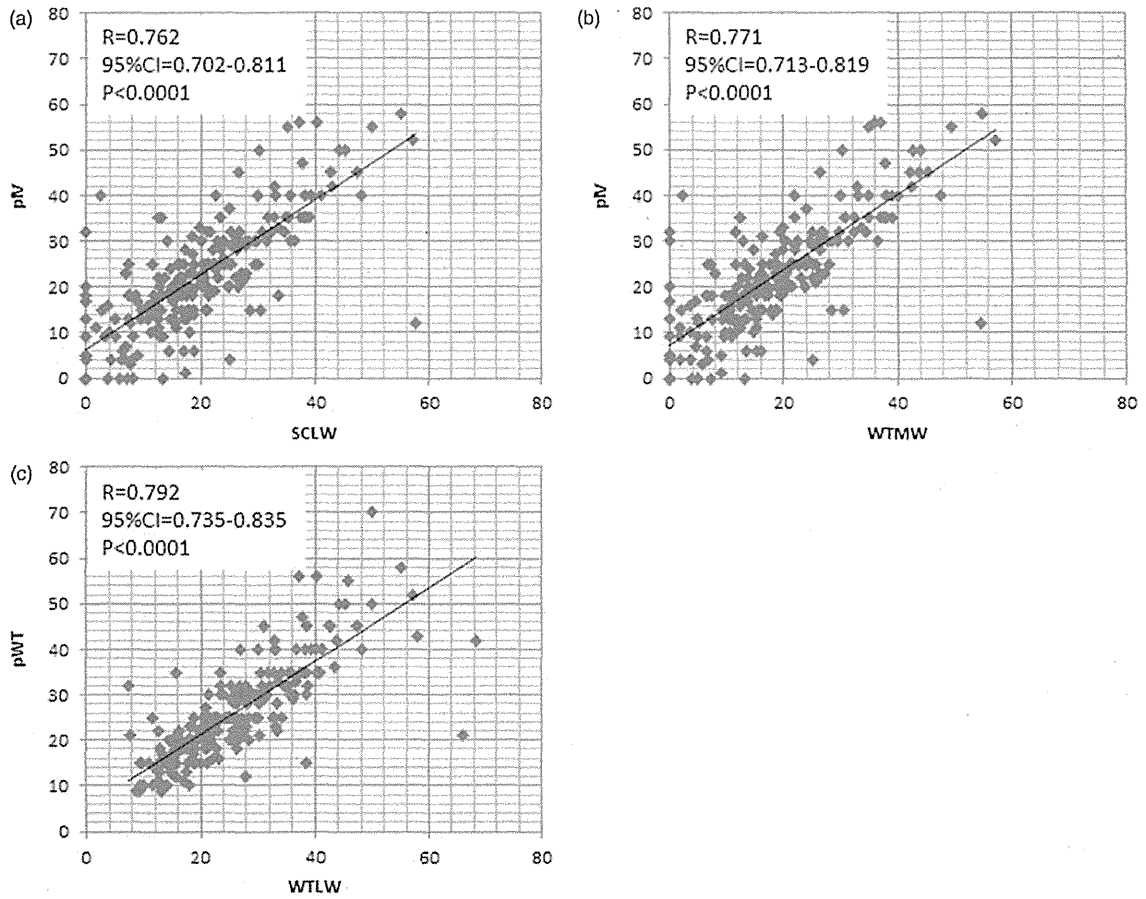


**Fig. 2.** Correlative graphs between radiological and pathological findings. There were significant correlations between SCLW and pIV ( $R = 0.762$ ,  $95\% \text{ CI} = 0.702\text{--}0.811$ ,  $P < 0.0001$ ) (a), WTMW and pIV ( $R = 0.771$ ,  $95\% \text{ CI} = 0.713\text{--}0.819$ ,  $P < 0.0001$ ) (b), and WTLW and pIV ( $R = 0.792$ ,  $95\% \text{ CI} = 0.735\text{--}0.835$ ,  $P < 0.0001$ ) (c), respectively. pIVS, pathologically confirmed invasion size; pWT, pathologically confirmed whole tumor size; SCLW, solid component size of lung windows setting; WTLW, whole tumor size of lung windows setting; WTMW, whole tumor size of mediastinal setting.

**Table 2.** Receiver operative characteristic area under the curve values of WTLW, SCLW, WTMW, and pIVS used to predict pathologic findings.

Variable	WTLW		SCLW		WTMW		pIVS	
	AUC (95% CI)	P value	AUC (95% CI)	P value	AUC (95% CI)	P value	AUC (95% CI)	P value
pN	0.711 (0.625–0.797)	<0.0001	0.796 (0.723–0.870)	<0.0001	0.809 (0.737–0.880)	<0.0001	0.788 (0.717–0.859)	<0.0001
Ly	0.685 (0.616–0.754)	<0.0001	0.793 (0.735–0.852)	<0.0001	0.801 (0.744–0.859)	<0.0001	0.772 (0.711–0.833)	<0.0001
V	0.646 (0.593–0.719)	<0.0001	0.766 (0.704–0.828)	<0.0001	0.769 (0.706–0.831)	<0.0001	0.777 (0.717–0.837)	<0.0001
pN or Ly or V	0.693 (0.623–0.762)	<0.0001	0.817 (0.761–0.873)	<0.0001	0.824 (0.769–0.879)	<0.0001	0.796 (0.733–0.855)	<0.0001
Well diff.	0.623 (0.551–0.695)	0.001	0.770 (0.710–0.830)	<0.0001	0.771 (0.711–0.832)	<0.0001	0.770 (0.709–0.830)	<0.0001

Ly, lymphatic invasion; pIVS, pathological invasion size; pN, pathological lymph node status; SCLW, solid component size of lung windows setting; V, vascular invasion; Well diff., well differentiated; WTLW, whole tumor size of lung windows setting; WTMW, whole tumor size of mediastinal setting.

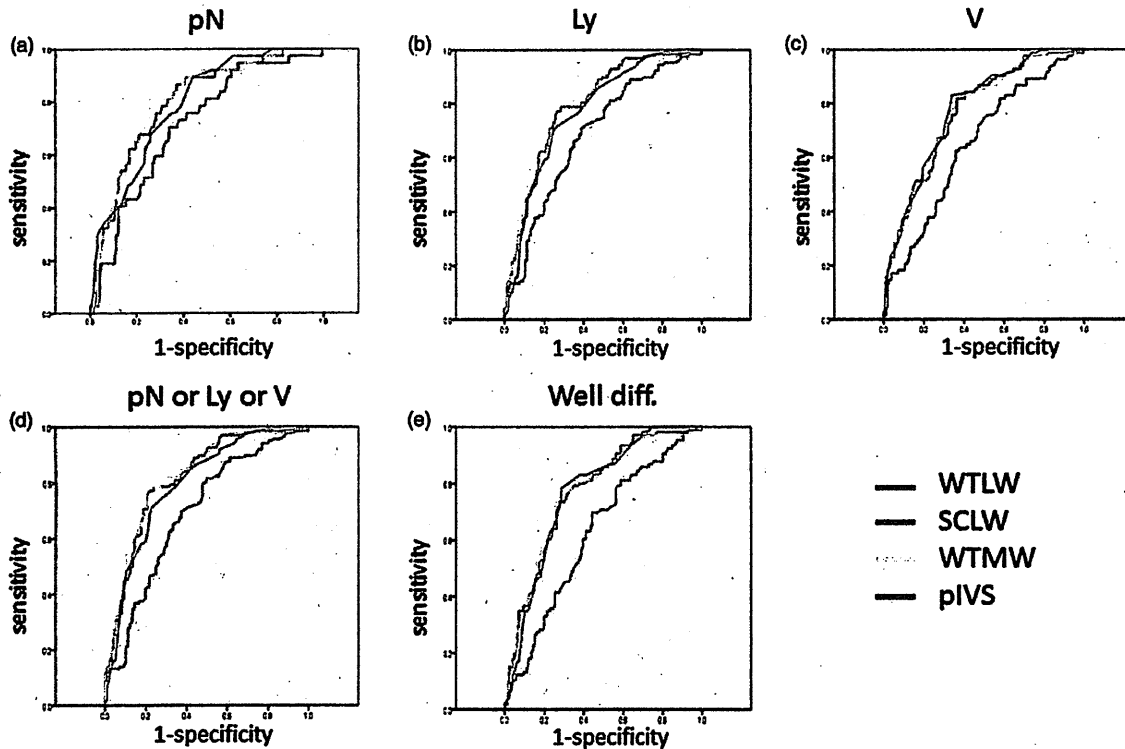


**Fig. 3.** Receiver operating characteristic area under the curve for detecting (a) pathological lymph node metastasis (pN), (b) lymphatic invasion (Ly), (c) vascular invasion (V), (d) high-grade malignancy (pN, VI, or PI), and (e) degree of differentiation for radiological whole and solid tumor sizes including WTLW, SCLW, and WTMW and pathological invasion area, pIVS. SCLW, solid component size of lung windows setting; WTLW, whole tumor size of lung windows setting; WTMW, whole tumor size of mediastinal setting.

whole tumor size that is WTLW for all subjects. The receiver operating characteristic curves of SCLW and WTMW were similar to that of pIVS that is pathological confirmed invasion area.

#### Survival significance

We assessed survival significance of preoperative radiological findings including WTLW, SCLW, and WTMW. Patients were categorized into radiological measurement of tumor size greater than 2 cm or those 2 cm or less according to WTLW, SCLW, and WTMW. There were significant differences in both the DFS and OS of this series according to SCLW ( $P=0.0001$  and  $P=0.023$ ) and WTMW ( $P<0.0001$  and  $P=0.008$ ), respectively (Fig. 4). Moreover, to find the most valuable and independent radiological prognostic factor including WTLW, SCLW, and WTMW as a candidate of next T factor, we performed multivariate analysis of DFS and OS. Table 3 revealed that WTMW (HR=0.72, 95% CI=0.58–0.90,  $P=0.004$  and HR=0.74, 95% CI=0.57–0.96,  $P=0.022$ , respectively) was the independent prognostic factor among

preoperative variables among age, sex, WTLW, and SCLW in this series.

#### Discussion

The frequency of identification of small lung cancers has increased since CT and enhanced scanning have become routine procedures. Small tumors, especially in lung adenocarcinomas, often contain GGO components as visualized on HRCT (2,7–9). Noguchi et al. first reported that type A and B small peripheral adenocarcinomas (localized bronchioloalveolar carcinoma without foci of active fibroblastic proliferation) showed no lymph node metastasis and a favorable prognosis (100% 5-year survival rate) (10). In 2011, new concepts were introduced including AIS and MIA. Because some of these cancers did not show growth for a long period, controversy remains as to how to manage subsolid nodules (11–14). Furthermore, both subsolid nodules and AIS have been discussed in relation to over diagnosis, which is defined as a diagnosis of lung cancer that would not lead to an individual's death because of the slow

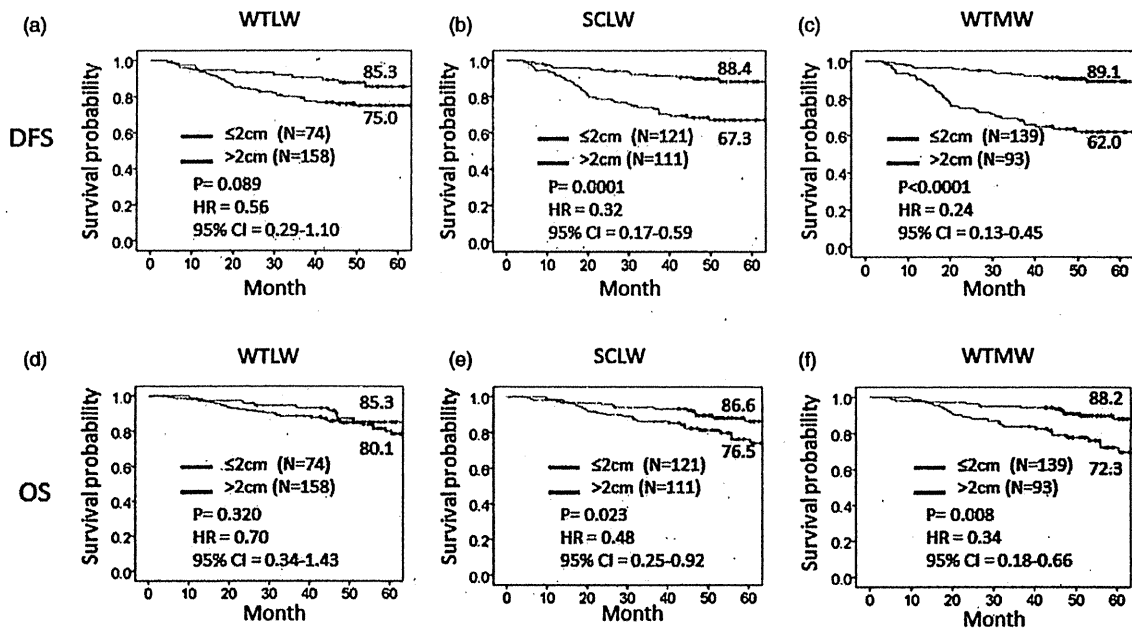


**Fig. 4.** Disease-free survival (DFS) and overall survival (OS) curves of patients according to tumor size on HRCT. (a) five-year DFS rate of 85.3% and 75.0% for a WTLW of 2.0 cm or less and greater than 2.0 cm, respectively ( $P=0.089$ ). (b) five-year DFS rate of 88.4% and 67.3% for a SCLW of 2.0 cm or less and greater than 2.0 cm, respectively ( $P=0.0001$ ). (c) five-year DFS rate of 89.1% and 62.0% for a WTMW of 2.0 cm or less and greater than 2.0 cm, respectively ( $P<0.0001$ ). (d) five-year OS rate of 85.2% and 80.1% for a WTLW of 2.0 cm or less and greater than 2.0 cm, respectively ( $P=0.320$ ). (e) five-year OS rate of 86.6% and 76.5% for a SCLW of 2.0 cm or less and greater than 2.0 cm, respectively ( $P=0.023$ ). (f) five-year OS rate of 88.2% and 72.3% for a WTLW of 2.0 cm or less and greater than 2.0 cm, respectively ( $P=0.008$ ). SCLW, solid component size of lung windows setting; WTLW, whole tumor size of lung windows setting; WTMW, whole tumor size of mediastinal setting.

**Table 3.** Multivariate analysis of DFS and OS.

Variable	Category	DFS			OS		
		HR	95% CI	P value	HR	95% CI	P value
Age (years)	<70						
	≥70	1.57	0.82–3.01	0.177	1.14	0.57–2.26	0.715
Sex	Men						
	Women	0.97	0.54–1.74	0.911	0.603	0.30–1.20	0.148
WTLW		0.94	0.89–1.00	0.040*	0.97	0.92–1.03	0.345
SCLW		0.82	0.66–1.01	0.067	0.80	0.62–1.03	0.078
WTMw		0.72	0.58–0.90	0.004*	0.74	0.57–0.96	0.022*

\*Statistically significant.

CI, confidence interval; DFS, disease-free survival; HR, hazard ratio; OS, overall survival; SCLW, solid component size of lung windows setting; WTLW, whole tumor size of lung windows setting; WTMW, whole tumor size of mediastinal setting.

growth rate and competing age-related risks for death (15–18).

The general concept of TNM classification by UICC is that “For consistency, in the TNM system, carcinoma in situ is categorized as Stage 0”, according to the 7<sup>th</sup> edition of the TNM Classification of Malignant

Tumours (19), which means AIS itself should not be used for staging grouping. However, clinical physicians specializing in lung cancer measure the tumor size by including the GGO components visualized on HRCT. On the basis of our hypothesis that the solid components, not the GGO components, of tumors as

visualized on HRCT, indicate malignancy and prognosis, we evaluated the role of solid tumor size (the size without the GGO component) in cases of lung adenocarcinoma.

First, we demonstrated that correlations between radiological findings including WTLW, SCLW, or WTMW, and pathological findings including pWT or pIVS. There were significant correlations between pIVS and SCLW or WTMW and between pWT and WTLW. Next we analyzed sensitivity and specificity of these radiological factors for predicting pathological malignant factors including lymph node involvement, lymphatic invasion, vascular invasion, and differentiation of the tumor. All receiver operating characteristic areas under the curves for predicting pN, Ly, V, high-grade malignancy (pN or Ly or V) and well differentiation were greater in the solid components size which is SCLW and WTMW than those for the whole tumor size which is WTLW. Because the range of mean radiological measurement of WTLW, SCLW and WTMW were from 1.87 to 2.59 cm in size and the cutoff point of 2 cm is also used as T factor. Finally, we analyzed each DFS and OS according to the cutoff point of 2 cm using whole and solid tumor sizes. Kaplan-Meier curves of both DFS and OS showed better division according to the solid components size, SCLW and WTMW, compared with the whole tumor size, WTLW. Moreover, multivariate analysis revealed that WTMW were identified as independent predictive factors for both DFS and OS. These results indicate that solid tumor size, not whole tumor size, more closely reflects the pathologic findings and those related to clinical tumor malignancy.

Several investigators have reported that the prognosis of patients with lung adenocarcinoma and a large GGO component visualized on HRCT was much better than that of patients with other adenocarcinoma types, irrespective of the maximal tumor dimension (20–23). In addition, JCOG0201, a multicenter prospective radiological study has examined the specificity, sensitivity, and accuracy of the radiologic diagnoses of lymphatic/vessel invasion and nodal involvement of clinical TINOM0 adenocarcinoma made according to the HRCT findings (24). Recently, a multicenter registration study demonstrated that solid tumor size on HRCT and maximum standardized uptake values on PET/CT has greater predictive value for high-grade malignancy and prognosis in clinical stage IA lung adenocarcinoma than that of whole tumor size (25). This final result indicated that using the solid tumor size is much simpler than using the GGO ratio; furthermore, the solid tumor size can be applied to the T descriptor in the TNM classification.

In this study, patients with lung adenocarcinoma were eligible for assessment and approximately one-third of the patients with whole tumors greater than

3 cm were included in final analysis. This confirmation of the significance of using the solid component for prognosis is consistent with previous studies using small-sized lung adenocarcinoma. Therefore, this result suggested that this concept of using solid tumor size can be applied to the T descriptor of TNM classification for larger tumors.

To the best of our knowledge, this is the first study demonstrating the correlation between radiological and pathological findings and the prognostic significance of solid tumor size in lung adenocarcinoma including tumors larger than 3 cm. However, there are several limitations in this study. First, this was a medium-size retrospective, single-institution analysis. Second, to clarify and simplify measuring the radiological and pathological size, we excluded lung adenocarcinoma with scattered invasive components which were slightly less than 10% of the population. It remains unclear whether we should count the largest scattered invasive components or the sum total of them. Third, we used two radiological measurements, SCLW and WTMW, in this analysis. Our results suggested that using WTMW counting for solid invasive components might be a better mediator for prognostic outcome of lung adenocarcinoma compared with SCLW, which is consistent with some of the previous. It remains unclear whether WTMW or SCLW should be a better predictor. Therefore, larger and multicenter studies using identical protocols are needed.

In conclusion, the predictive values of solid tumor size visualized on HRCT especially in mediastinal windows for pathologic high-grade malignancy and prognosis in patients with lung adenocarcinoma were greater than those of the whole tumor size. We recommend that the solid tumor size be used to determine the T descriptor in the TNM classification of lung tumor and be defined as the true tumor size in cases of lung adenocarcinoma with a GGO component visualized on HRCT.

#### Acknowledgements

We are indebted to Professor James M. Vardaman of Waseda University and Professor J Patrick Barron, Chairman of the Department of International Medical Communications of Tokyo Medical University, for their editorial review of the English manuscript.

#### Conflict of interest

None declared.

#### Funding

This study was supported by a Grant-in-Aid for Scientific Research, Japan Society for the Promotion of Science (24592104), Ministry of Education, Culture, Sports, Science and Technology, Japan.

**References**

1. Aberle DR, Adams AM, Berg CD, et al. Reduced lung-cancer mortality with low-dose computed tomographic screening. *N Engl J Med* 2011;365:395-409.
2. Nakata M, Saeki H, Takata I, et al. Focal ground-glass opacity detected by low-dose helical CT. *Chest* 2002;121:1464-1467.
3. Travis WD, Brambilla E, Noguchi M, et al. International Association for the Study of Lung Cancer/American Thoracic Society/European Respiratory Society: international multidisciplinary classification of lung adenocarcinoma: executive summary *Proc Am Thorac Soc* 2011;8:381-385.
4. Lee HJ, Goo JM, Lee CH, et al. Predictive CT findings of malignancy in ground-glass nodules on thin-section chest CT: the effects on radiologist performance. *Eur Radiol* 2009;19:552-560.
5. Goldstraw P, Crowley J, Chansky K, et al. The IASLC Lung Cancer Staging Project: proposals for the revision of the TNM stage groupings in the forthcoming (seventh) edition of the TNM Classification of malignant tumours. *J Thorac Oncol* 2007;2:706-714.
6. Travis WD, Brambilla E, Muller-Hermelink H, et al. *World Health Organization Classification of Tumours: Pathology & Genetics Tumours of the Lung, Pleura, Thymus and Heart*, 3rd edn. Lyon: IARC Press, 2004.
7. Okada M, Koike T, Higashiyama M, et al. Radical sublobar resection for small-sized non-small cell lung cancer: a multicenter study. *J Thorac Cardiovasc Surg* 2006;132:769-775.
8. Nakayama H, Yamada K, Saito H, et al. Sublobar resection for patients with peripheral small adenocarcinomas of the lung: surgical outcome is associated with features on computed tomographic imaging. *Ann Thorac Surg* 2007;84:1675-1679.
9. Suzuki K, Kusumoto M, Watanabe S, et al. Radiologic classification of small adenocarcinoma of the lung: radiologic-pathologic correlation and its prognostic impact. *Ann Thorac Surg* 2006;81:413-419.
10. Noguchi M, Morikawa A, Kawasaki M, et al. Small adenocarcinoma of the lung. Histologic characteristics and prognosis. *Cancer* 1995;75:2844-2852.
11. Kodama K, Higashiyama M, Yokouchi H, et al. Natural history of pure ground-glass opacity after long-term follow-up of more than 2 years. *Ann Thorac Surg* 2002;73:386-92; discussion 92-93.
12. Takashima S, Maruyama Y, Hasegawa M, et al. CT findings and progression of small peripheral lung neoplasms having a replacement growth pattern. *Am J Roentgenol* 2003;180:817-826.
13. Hiramatsu M, Inagaki T, Matsui Y, et al. Pulmonary ground-glass opacity (GGO) lesions-large size and a history of lung cancer are risk factors for growth. *J Thorac Oncol* 2008;3:1245-1250.
14. Sawada S, Komori E, Nogami N, et al. Evaluation of lesions corresponding to ground-glass opacities that were resected after computed tomography follow-up examination. *Lung Cancer* 2009;65:176-179.
15. Henschke CI, Yankelevitz DF, Mirtcheva R, et al. CT screening for lung cancer: frequency and significance of part-solid and nonsolid nodules. *Am J Roentgenol* 2002;178:1053-1057.
16. Toyoda Y, Nakayama T, Kusunoki Y, et al. Sensitivity and specificity of lung cancer screening using chest low-dose computed tomography. *Br J Cancer* 2008;98:1602-1607.
17. Jett JR. Limitations of screening for lung cancer with low-dose spiral computed tomography. *Clin Cancer Res* 2005;11:4988s-4992s.
18. Goo JM, Park CM, Lee HJ. Ground-glass nodules on chest CT as imaging biomarkers in the management of lung adenocarcinoma. *Am J Roentgenol* 2011;196:533-543.
19. Sobin LH, Gospodarowicz MK, Wittekind C. *TNM Classification of Malignant Tumours*. Oxford: John Wiley & Sons, Ltd., 2009.
20. Aoki T, Tomoda Y, Watanabe H, et al. Peripheral lung adenocarcinoma: correlation of thin-section CT findings with histologic prognostic factors and survival. *Radiology* 2001;220:803-809.
21. Suzuki K, Asamura H, Kusumoto M, et al. "Early" peripheral lung cancer: prognostic significance of ground glass opacity on thin-section computed tomographic scan. *Ann Thorac Surg* 2002;74:1635-1639.
22. Ohde Y, Nagai K, Yoshida J, et al. The proportion of consolidation to ground-glass opacity on high resolution CT is a good predictor for distinguishing the population of non-invasive peripheral adenocarcinoma. *Lung Cancer* 2003;42:303-310.
23. Tsutani Y, Miyata Y, Yamanaka T, et al. Solid tumors versus mixed tumors with a ground-glass opacity component in patients with clinical stage IA lung adenocarcinoma: Prognostic comparison using high-resolution computed tomography findings. *J Thorac Cardiovasc Surg* 2013;146:17-23.
24. Suzuki K, Koike T, Asakawa T, et al. A prospective radiological study of thin-section computed tomography to predict pathological noninvasiveness in peripheral clinical IA lung cancer (Japan Clinical Oncology Group 0201). *J Thorac Oncol* 2011;6:751-756.
25. Tsutani Y, Miyata Y, Nakayama H, et al. Prognostic significance of using solid versus whole tumor size on high-resolution computed tomography for predicting pathologic malignant grade of tumors in clinical stage IA lung adenocarcinoma: a multicenter study. *J Thorac Cardiovasc Surg* 2012;143:607-612.



# Ultra-low-dose CT of the Lung:

## *Effect of Iterative Reconstruction Techniques on Image Quality*

Masahiro Yanagawa, MD, PhD, Tomoko Gyobu, MD, Ann N. Leung, MD, Misa Kawai, MD, Yutaka Kawata, MD, Hiromitsu Sumikawa, MD, PhD, Osamu Honda, MD, PhD, Noriyuki Tomiyama, MD, PhD

**Rationale and Objectives:** To compare quality of ultra-low-dose thin-section computed tomography (CT) images of the lung reconstructed using model-based iterative reconstruction (MBIR) and adaptive statistical iterative reconstruction (ASIR) to filtered back projection (FBP) and to determine the minimum tube current-time product on MBIR images by comparing to standard-dose FBP images.

**Materials and Methods:** Ten cadaveric lungs were scanned using 120 kVp and four different tube current-time products (8, 16, 32, and 80 mAs). Thin-section images were reconstructed using MBIR, three ASIR blends (30%, 60%, and 90%), and FBP. Using the 8-mAs data, side-to-side comparison of the four iterative reconstruction image sets to FBP was performed by two independent observers who evaluated normal and abnormal findings, subjective image noise, streak artifact, and overall image quality. Image noise was also measured quantitatively. Subsequently, 8-, 16-, and 32-mAs MBIR images were compared to standard-dose FBP images. Comparisons of image sets were analyzed using the Wilcoxon signed rank test with Bonferroni correction.

**Results:** At 8 mAs, MBIR images were significantly better ( $P < .005$ ) than other reconstruction techniques except in evaluation of interlobular septal thickening. Each set of low-dose MBIR images had significantly lower ( $P < .001$ ) subjective and objective noise and streak artifacts than standard-dose FBP images. Conspicuity and visibility of normal and abnormal findings were not significantly different between 16-mAs MBIR and 80-mAs FBP images except in identification of intralobular reticular opacities.

**Conclusions:** MBIR imaging shows higher overall quality with lower noise and streak artifacts than ASIR or FBP imaging, resulting in nearly 80% dose reduction without any degradations of overall image quality.

**Key Words:** Radiation dose reduction; model-based iterative reconstruction; adaptive statistical iterative reconstruction; filtered back projection; image quality.

©AUR, 2014

The increase of the radiation dose delivered in computed tomography (CT) has recently been a problem. Because there is a trade-off between image quality and radiation dose on CT, however, it is not always appropriate to decrease radiation dose on CT. Iterative reconstruction algorithms for CT have been developed by multiple equipment manufacturers to reduce image noise associated with radiation dose reduction (1–8). Adaptive statistical iterative reconstruction (ASIR) and model-based iterative reconstruction (MBIR) are types of iterative reconstruction algorithms available on clinical settings. The ASIR technique models photon and electronic noise statistics; by partially correcting for fluctuations in projection measurements due to limited photon statistics, ASIR enables a time-efficient reduc-

tion in pixel variance that is statistically unlikely to be representative of anatomic features resulting in a reduction of image noise with no decrement in spatial resolution (9). In clinical practice, ASIR is typically used in combination with the standard filtered back projection (FBP) reconstruction to create blended images. As compared to ASIR, MBIR is a more mathematically complex and time-consuming technique as it models not only system statistics but also system optics (10). Phantom experiments show that MBIR has potential to improve spatial resolution and allow further reductions in image noise (9). To date, few studies have evaluated CT image quality of the lung using MBIR (10–14). Thus, unlike FBP and ASIR, MBIR technique might have the potential not to degrade image quality even under the extreme dose reduction. McCollough et al. (15) reported that the advances in data acquisition, image reconstruction, and optimization processes that were identified by consensus as being necessary to achieve submillisievert-dose CT examinations. It is expected that MBIR might be one of techniques to enable a submillisievert-dose CT. The present study was performed using cadaveric lung models that can provide multiple acquisitions to determine the minimum tube current-time product at which image quality of a low-dose MBIR study is comparable to that of a standard-dose FBP study. The aim of this present study was two-fold: to compare quality of ultra-low-dose

Acad Radiol 2014; 21:695–703

From the Department of Diagnostic Radiology, Stanford University School of Medicine, 1201 Welch Rd, Stanford, CA 94305 (M.Y., A.N.L.); Department of Radiology, Osaka University Graduate School of Medicine, Suita, Osaka, Japan (M.Y., T.G., M.K., H.S., O.H., N.T.); and Department of Radiology, Osaka Rosai Hospital, Sakai, Osaka, Japan (Y.K.). Received December 2, 2013; accepted January 31, 2014. All authors declare that there is no conflict of interest. **Address correspondence to:** M.Y. e-mail: masayana@stanford.edu or m-yanagawa@radiol.med.osaka-u.ac.jp

©AUR, 2014

<http://dx.doi.org/10.1016/j.acra.2014.01.023>

thin-section CT images of the lung reconstructed using MBIR and ASIR to FBP and to determine the minimum tube current–time product at which image quality of an MBIR study is comparable to that of a standard-dose FBP.

## MATERIALS AND METHODS

### Cadaveric Lungs and Imaging

We obtained approval from our internal Ethics Review Board. Informed consent was obtained for the use of patient biomaterial and for retrospective review of patient records and images. Ten cadaveric lungs were inflated and fixed by the method of Heitzman (16). These lungs were distended through the main bronchus with fixative fluid that contained polyethylene glycol 400, 95% ethyl alcohol, 40% formalin, and water in the proportions of 10:5:2:3. The specimens were immersed in fixative for 2 days and the lungs were then air dried. The pathologic diagnoses of these 10 lungs were usual interstitial pneumonia ( $n = 1$ ), diffuse alveolar damage ( $n = 1$ ), diffuse panbronchiolitis ( $n = 1$ ), pneumonia ( $n = 2$ ), emphysema ( $n = 1$ ), diffuse alveolar hemorrhage ( $n = 1$ ), metastatic disease ( $n = 2$ ), and lymphangitic carcinomatosis ( $n = 1$ ).

The 10 lungs were scanned on a multi-detector row CT (MDCT) scanner (Discovery CT750HD; GE Healthcare Technologies, Milwaukee, WI). CT protocol was as follows: detector collimation, 0.625 mm; detector pitch, 0.984; gantry rotation period, 0.4 seconds; matrix size,  $512 \times 512$  pixels; 30-cm scan length; x-ray voltage, 120 kVp; tube current, 20, 40, 80, and 200 mA; and non-high-resolution mode with 984 views per rotation. Both ASIR and MBIR are part of the commercially available package implemented on the control panel of the CT scanner.

Axial thin-section CT images of 0.625 mm thickness and 20 cm field of view were reconstructed with MBIR, ASIR (30%, 60%, and 90% [represented as ASIR<sub>30</sub>, ASIR<sub>60</sub>, and ASIR<sub>90</sub>]), and FBP. The voxel dimensions of CT image are  $0.391 \times 0.391 \times 0.625$  mm. A high-spatial-frequency algorithm was used in ASIR and FBP; however, there was no concept of reconstruction algorithm in MBIR. Based on lung cancer screening literature (17) that defines a tube current–time product of 40 mAs as “low dose”, we use the term “ultra-low-dose” CT to refer to studies acquired with tube current–time products  $\leq 20$  mAs and result in an effective dose of  $< 1$  mSv.

### Subjective Image Analysis

Three to four cross-sectional levels with the most conspicuous CT findings were chosen from each cadaveric lung by the principal investigator (M.Y., with 12 years of experience): three images were selected for seven lungs and four images for the remaining three lungs. There were a total of 264 images, that is, 33 sets of 8 image series (8-mAs, 16-mAs, and 32-mAs MBIR, 8-mAs ASIR<sub>30</sub>, 8-mAs ASIR<sub>60</sub>, 8-mAs ASIR<sub>90</sub>, and 8-mAs and 80-mAs FBP).

TABLE 1. Radiation Dose Descriptions

	Low Dose			Standard Dose
	8 mAs	16 mAs	32 mAs	80 mAs
CTDIvol (mGy)	0.65	1.30	2.59	6.49
DLP (mGy-cm)	22.15	44.30	88.60	221.50
ED (mSv)	0.31	0.62	1.24	3.10

CTDIvol, computed tomography dose index volume; DLP, dose-length product; ED, effective dose.

Two independent chest radiologists (M.K. and Y.K., with 8 years of experience each) without prior knowledge of the pathologic diagnoses, image acquisition parameters, or iterative reconstruction techniques reviewed the 264 images on a 5-megapixel 21-in monochrome liquid-crystal display monitor. All images were displayed at a window level of  $-700$  Hounsfield units (HU) and a window width of 1200 HU. In the first step, 8-mAs MBIR and 8-mAs ASIR were compared to 8-mAs FBP. Approximately 1 month later, in the second step, 8-mAs, 16-mAs, and 32-mAs MBIR were compared to 80-mAs FBP.

The two observers compared the conspicuity and visibility of normal (central and peripheral vessels, central and peripheral airways, and interlobar fissures) and abnormal (ground-glass opacity [GGO], consolidation, nodules, interlobular septal thickening, intralobular reticulation, cyst, and bronchiectasis) CT findings using a five-point scale as compared to the FBP image: (1) an unacceptable image on which it was more difficult to detect and/or visualize findings in whole lung; (2) an inferior image on which it was more difficult to detect and/or visualize findings in at least one area of the lung; (3) an image comparable to the FBP image; (4) a superior image on which it was easier to detect and/or visualize findings in at least one area of the lung; and (5) an excellent image on which it was easier to detect and/or visualize findings in whole lung. Subjective visual noise and streak artifact were also graded on a five-point comparative scale: (1) noise/artifact significantly worse, nondiagnostic; (2) noise/artifact worse; (3) similar noise/artifact compared to image of FBP; (4) noise/artifact improved; and (5) noise/artifact significantly improved, almost nondetectable. Overall image quality was finally graded on a five-point scale: (1) unacceptable, nondiagnostic; (2) inferior; (3) comparable to the FBP image; (4) better; and (5) excellent. If there were different scores between two observers, final evaluation was decided by an adjudicator (H.S., with 13 years of experience).

### Objective Image Analysis

Quantitative noise measurements were calculated by measuring the standard deviation (SD) in a circular region of interest (ROI) defined by an electric cursor, using free software (ImageJ version 1.37v; NIH, Bethesda, MD; for further information regarding ImageJ software, see <http://rsb.info.nih.gov/ij/index.html>). Quantitative noise measurements

TABLE 2. Comparison among FBP, ASIR, and MBIR on Ultra-low-dose (8 mAs) CT

Reconstruction technique	Normal Findings			Abnormal Findings			Other Findings		Overall Image Quality
	Central Vessels and Airways	Peripheral Vessels and Airways	Interlobar Fissures	Nodules	GGO	ISP	Image Noise	Streak Artifact	
MBIR	4.83 ± 0.07	4.68 ± 0.09	4.75 ± 0.11	4.96 ± 0.04	4.84 ± 0.07	4.19 ± 0.16	5.00 ± 0.00	5.00 ± 0.00	4.97 ± 0.03
ASIR <sub>90</sub>	4.06 ± 0.11	4.04 ± 0.07	4.00 ± 0.13	4.00 ± 0.05	4.16 ± 0.07	3.88 ± 0.09	4.21 ± 0.07	4.03 ± 0.12	4.55 ± 0.09
ASIR <sub>60</sub>	3.52 ± 0.09	3.32 ± 0.09	3.19 ± 0.10	3.39 ± 0.09	3.84 ± 0.07	3.31 ± 0.12	3.73 ± 0.08	3.45 ± 0.09	3.55 ± 0.09
ASIR <sub>30</sub>	3.00 ± 0.00	3.00 ± 0.00	3.00 ± 0.00	3.04 ± 0.04	3.04 ± 0.04	3.00 ± 0.00	3.03 ± 0.03	3.00 ± 0.00	3.00 ± 0.00
FBP	3.00 ± 0.00	3.00 ± 0.00	3.00 ± 0.00	3.00 ± 0.00	3.00 ± 0.00	3.00 ± 0.00	3.00 ± 0.00	3.00 ± 0.00	3.00 ± 0.00
Pairwise comparison ( <i>P</i> <sup>*</sup> )									
MBIR versus ASIR <sub>90</sub>	<.001	<.001	.005	<.001	<.001	.962	<.001	<.001	<.001
ASIR <sub>60</sub>	<.001	<.001	<.001	<.001	<.001	.002	<.001	<.001	<.001
ASIR <sub>30</sub>	<.001	<.001	<.001	<.001	<.001	<.001	<.001	<.001	<.001
FBP	<.001	<.001	<.001	<.001	<.001	<.001	<.001	<.001	<.001
ASIR <sub>90</sub> versus ASIR <sub>60</sub>	<.001	<.001	<.001	<.001	.084	.005	<.001	<.001	<.001
ASIR <sub>30</sub>	<.001	<.001	<.001	<.001	<.001	<.001	<.001	<.001	<.001
FBP	<.001	<.001	<.001	<.001	<.001	<.001	<.001	<.001	<.001
ASIR <sub>60</sub> versus ASIR <sub>30</sub>	<.001	.026	.825	.006	<.001	.197	<.001	<.001	<.001
FBP	<.001	.026	.825	.003	<.001	.197	<.001	<.001	<.001
ASIR <sub>30</sub> versus FBP	1.000	1.000	1.000	1.000	1.000	1.000	1.000	1.000	1.000

ASIR, adaptive statistical iterative reconstruction; GGO, ground-glass opacity; ISP, interlobular septal thickening; FBP, filtered back projection; MBIR, model-based iterative reconstruction. Data are presented as mean ± standard deviation. Data of the subjective image analysis were statistically analyzed using the Wilcoxon signed rank tests with a Bonferroni correction applied for multiple comparisons. *P*<sup>\*</sup> is a Bonferroni-corrected *P* value. *P*<sup>\*</sup> value <.05 was considered to be significant.

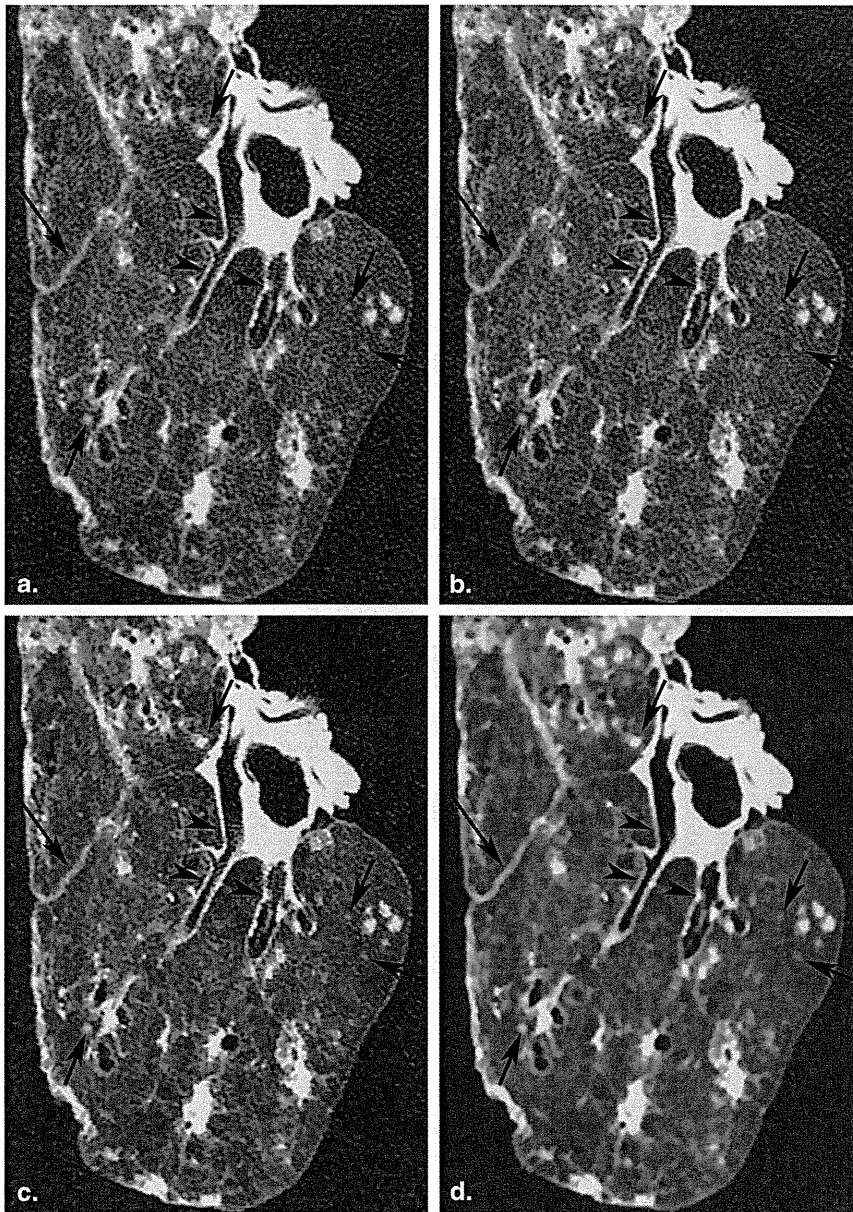


**Figure 1.** Ultra-low-dose (8 mAs) thin-section computed tomographic images of a cadaveric lung with diffuse panbronchiolitis show serial improvement in image noise and streak artifacts in following ascending order: FBP (a), ASIR<sub>30</sub> (b), ASIR<sub>90</sub> (c), and MBIR (d). With almost no perceptible noise or streak artifact on MBIR image, conspicuity and visibility of the fissure (*long arrow*), small nodules (*short arrows*), and bronchial walls (*arrowheads*) are improved as compared to FBP or ASIR blends. Note the blotchy pixilated appearance of the MBIR images. ASIR, adaptive statistical iterative reconstruction; FBP, filtered back projection; MBIR, model-based iterative reconstruction.

were obtained in the air adjacent to the lung specimen (18,19). An ROI (200 mm<sup>2</sup>) was placed in four homogeneous parts of an image and was confirmed to be in exactly the same location on each image of a series by a collaborator (T.G., with 8 years of experience). Average values of SD were analyzed statistically.

### Statistical Analysis

All statistical analyses were performed using commercially available software (MedCalc version 12.3.0.0 statistical software; Frank Schoonjans, Mariakerke, Belgium). Agreement between two observers in each evaluated category of CT findings was evaluated using the  $\kappa$  statistic and classified as poor ( $\kappa = 0.00$ – $0.20$ ), fair ( $\kappa = 0.21$ – $0.40$ ), moderate ( $\kappa = 0.41$ – $0.60$ ), good ( $\kappa = 0.61$ – $0.80$ ), or excellent ( $\kappa = 0.81$ – $1.00$ ).

Data of the subjective image analysis were statistically analyzed using the Wilcoxon signed rank tests, which was conducted with Bonferroni correction applied for multiple comparisons. On the other hand, data of the objective image analysis were statistically analyzed using repeated measures analysis of variance pairwise comparison methods (Student's paired *t* test) with Bonferroni correction. A Bonferroni-corrected *P* value of  $<0.05$  was considered significant.

## RESULTS

### Radiation Doses

Radiation dose measurements associated with low-dose (8, 16, and 32 mAs) and standard-dose (80 mAs) techniques